 DOI: 10.31276/VJSTE.2025.0001

Synthesis of AuCu nanoalloy and investigation on its electrocatalytic proton reduction and CO_2 reduction activity

Tran Duc Tien, Le Thi Ly, Nguyen Ngoc Duc, Nguyen Thi Quyen, Tran Dinh Phong*

University of Science and Technology of Hanoi, Vietnam Academy of Science and Technology, 18 Hoang Quoc Viet Street, Nghia Do Ward, Cau Giay District, Hanoi, Vietnam

Received 12 January 2025; revised 4 February 2025; accepted 27 February 2025

Abstract:

Identifying efficient catalysts for the H_2 evolution reaction and CO_2 reduction, which can operate at low overpotential in a neutral or near-neutral pH aqueous solution, represents a significant challenge. This work reports the synthesis of an AuCu nanoalloy in the form of spherical nanoparticles with an average size of ~16.7±0.3 nm. The morphology, crystal structure, and chemical composition of AuCu nanoparticles were characterised by scanning electron microscopy (SEM), transmission electron microscopy (TEM), high resolution - high angle annular dark field - scanning transmission electron microscopy (HR-HAADF-STEM), and energy dispersive X-ray (EDX) analysis. The use of AuCu nanoparticles as a catalyst for the H_2 evolution and CO_2 reduction reactions in a 0.1 M $KHCO_3$ (pH 6.8) solution was investigated. It was found that AuCu nanoparticles catalysed the reduction of CO_2 to CH_4 at a low cathodic potential of -0.2 V *vs.* Reversible hydrogen electrode (RHE) with a Faradaic efficiency of 7.1%. However, at low cathodic potentials ranging from -0.2 to -0.5 V *vs.* RHE, H_2 evolution was more favourable than CO_2 reduction reactions. Conversely, at higher cathodic potentials, *e.g.* -0.6 V *vs.* RHE, the reduction of CO_2 to CO was more favourable. The AuCu nanoparticles demonstrate superior CO_2 reduction selectivity compared to Au and Cu nanoparticle catalysts. A discussion on potential reaction pathways contributing to the CO_2 reduction selectivity is also proposed.

Keywords: **catalysis, copper, CO_2 reduction, fuels, gold, nanocatalyst**.

Classification numbers: **2.1, 2.2, 2.3**

1. Introduction

Water electrolysis or photoelectrolysis (also called water splitting) is considered as an attractive technology for the large-scale production of green H_2 [1, 2]. It consists of two half-reactions, namely the hydrogen evolution reaction and the oxygen evolution reaction, which have sluggish kinetics due to their multiple electron and proton nature. To accelerate these reactions, efficient catalysts are required. For instance, Pt is known to be the most efficient and stable H_2 evolution catalyst, but its extremely low abundance in the Earth's crust limits its potential industrial use [3]. To address this issue, several attractive alternatives to Pt catalysts have been developed, such as transition metal sulfides [4-9], transition metal phosphides [10, 11], or coordination complexes of transition metals [12, 13]. In our previous works, we have demonstrated that gold nanoparticles (Au NPs) [14, 15] and silver nanoparticles (Ag NPs) [16] were excellent catalysts for H_2 evolution in an acidic solution, e.g. 0.5 M H_2SO_4. However, in a neutral pH electrolyte, e.g. pH 7 phosphate buffer, these catalysts showed much lower catalytic performance. In contrast, Cu/Cu_2O nanoparticles, generated via an electrochemical reduction or a photoelectrochemical reduction of Cu_2O thin film, exhibited attractive catalytic activity in the pH 7 phosphate buffer [17].

Beyond water electrolysis producing green H_2, the idea of coupling water oxidation with CO_2 reduction has been initiated [18, 19]. By doing so, the greenhouse gas CO_2 can be reduced into CO, HCOOH, CH_3COOH, CH_4, CH_3OH, which can subsequently be used either as chemical stocks or fuels. In comparison to the H_2 evolution reaction, CO_2 reduction reactions have almost comparable equilibrium thermodynamic potentials. Therefore, the hydrogen

*Corresponding author: Email: tran-dinh.phong@usth.edu.vn

evolution reaction always competes with the CO_2 reduction reaction. In principle, due to its faster kinetics, the hydrogen evolution reaction usually prevails over CO_2 reduction reactions. In this context, significant efforts are being mobilised by the scientific community to identify catalysts that offer high CO_2 reduction selectivity versus H_2 evolution.

Among reported CO_2 reduction catalysts, the Cu catalyst is the most attractive one as it can offer a wide range of products from C_1 like CO, HCOOH, CH_4, CH_3OH to C_{2+} like CH_3COOH, HOOC-COOH, C_2H_4 …[20]. However, it is still not clear which structural features will affect its product selectivity. In our recent work, we demonstrated that CuO nanoparticles were an attractive catalyst for CO_2 reduction in a $KHCO_3$ electrolyte solution showing high HCOOH production selectivity with a Faradaic efficiency of 26% at -0.9 V *vs.* RHE [21]. In the group IB, Au [22] and Ag [23] were also reported to be active catalysts for the CO_2 reduction into CO.

To tune CO_2 reduction selectivity, a potential strategy is to create bimetallic catalysts. It was proposed that the bimetallic catalyst surface could adjust the adsorption of intermediates (thus altering the reaction pathways), generate more catalytically active sites, and even avoid catalyst poisoning [20, 24]. M.L. Frisch, et al. (2023) [25] demonstrated the superior CO_2 reduction selectivity versus H_2 evolution of a CuAg NPs bimetallic catalyst over monometallic Cu NPs. X. Ma, et al. (2020) [26] demonstrated superior CO_2 to CO reduction selectivity of a core@shell structure $AuCu_3$@Au NPs catalyst compared to the Au NPs catalyst, wherein the $AuCu_3$ core was proposed to reduce the absorption energy of [Au-COOH]* and [Au-CO]* intermediates. J. Huang, et al. (2020) [27] reported on a bimetallic AuCu NPs with an Au-rich core and a Cu-rich shell, showing outstanding CO_2-to-C_2H_4 reduction selectivity with a Faradaic yield of ~20%.

Herein, we report on the synthesis of an AuCu nanoalloy in the form of spherical nanoparticles (hereafter denoted as AuCu NPs) and investigate its electrochemical catalytic activity for H_2 evolution and CO_2 reduction in an aqueous pH-neutral electrolyte solution. We demonstrate the superior CO_2 reduction selectivity of AuCu NPs compared to Au NPs and Cu NPs catalysts. The potential mechanism by which the AuCu NPs catalyst promotes CO_2 reduction and inhibits H_2 evolution is also discussed.

2. Experimental section

2.1. Synthesis of AuCu nanoparticles

Deionised water (DI) was degassed by N_2 flux to remove dissolved oxygen before being used as the solvent for reactions. In a typical synthesis, 500 ml of $CuCl_2$ 0.01 M solution in DI water and 500 ml of $HAuCl_4$ 0.01 M solution in DI water were mixed. The mixture was stirred under N_2 flux and heated to 95°C. Then, 4 ml of trisodium citrate 0.1 M solution was added dropwise to the solution. After 5 minutes, 1.5 ml of hydrazine was added, and the reaction mixture was stirred for a further 30 minutes. Once the reaction was complete, the mixture was allowed to cool naturally to room temperature. AuCu nanoparticles (CuAu NPs), appearing as a dark brown suspension, were collected by centrifugation and thoroughly washed three times with DI water. Finally, they were re-dispersed in 3 ml of DI at a concentration of 0.435 $g.l^{-1}$ in a vial under N_2 atmosphere prior to use for characterisation or CO_2 reduction catalysis.

The same process was used to synthesise Au NPs and Cu NPs using only the $HAuCl_4$ precursor or $CuCl_2$ precursor, respectively.

2.2. Characterisation

The UV-Vis spectrum was collected using a Cary UV-Vis Compact instrument. The shape, size, and crystallinity of the AuCu NPs were examined by high-resolution HAADF-STEM (JEM, ARM200F microscope, operating at 200 kV, point resolution of 0.19 nm). TEM grids were prepared by casting a drop of the AuCu NPs suspension onto a copper grid (400 hexagonal meshes, carbon-coated). The grids were then dried under vacuum for at least one night before being introduced into the microscopy chamber.

2.3. Electrochemical assay

A 100-ml AuCu NPs solution with a concentration of 0.435 $g.l^{-1}$ was directly used as the catalyst ink and drop-casted onto a 0.283 cm^2 graphite substrate. The resultant catalyst electrode was dried at 40°C for 10 minutes.

The electrochemical assay was conducted using a Biologic Instrument SP200 potentiostat. A conventional three-electrode configuration was used with the catalyst working electrode, an Ag/AgCl 3M KCl reference electrode, and a Pt plate counter electrode. The electrolyte was a 0.1 M $KHCO_3$ solution at pH 6.8, saturated with CO_2 gas.

A linear sweep voltammogram (LSV) was recorded with a slow potential scan rate of 2 $mV.s^{-1}$. Bulk electrolysis was conducted at different constant potentials, ranging from -0.2 V to -0.9 V *vs.* RHE in a gas-tight two-compartment H-cell. After the 2-hour bulk electrolysis, gas products in the headspace of the H-cell were quantified using gas chromatography (GC). GC analysis was conducted using a PerkinElmer Clarus 690 instrument. 100 µl of the gas sample was injected by a gas-tight glass syringe into a Restek ShinCarbon ST 100/120 column operated at 90°C. The carrier gas flow was set at 12 $ml.min^{-1}$, the thermal conductivity detector (TCD) was operated at 200°C, and the flame ionisation detector (FID) was operated at 400°C. The H_2 calibration curve was built using a Pt catalyst electrode that generated H_2 at a constant current of 1 or 3 mA in 0.5 M H_2SO_4 in the same electrolysis cell. The calibration curve for CO was built using a CO standard gas with concentrations ranging from 0.1 to 1%. CH_4 was quantified by comparison with a 0.5% CH_4 standard gas. The quantification of formate and acetate was conducted with a Dionex Integrion high-performance ion chromatography (IC) system. DI water, used as the mobile phase, was set at a flow rate of 1 $ml.min^{-1}$. The calibration curve was built using Sigma-Aldrich formate and acetate standard solutions (1000 ppm).

3. Results and discussion

AuCu nanoparticles, referred to as AuCu NPs, were synthesised via the co-reduction of Cu^{II} and Au^{III} salts using hydrazine as the reducing agent in the presence of a citrate surfactant. By employing the same synthesis method, it was possible to prepare Cu NPs and Au NPs when using only the Cu^{II} or Au^{III} precursor, respectively. These Cu NPs and Au NPs were used as reference samples to discuss the physicochemical properties of AuCu NPs. TEM analysis showed the aggregation of small AuCu NPs, with an average particle size of ~16.7±0.3 nm (Fig. 1A). The size distribution was rather narrow (Fig. 1, inset). In solution with DI water as the solvent, these CuAu NPs exhibited similar plasmonic absorption to that of Au NPs, with an absorption maximum at ~528 nm (Fig. 1B).

As expected, no plasmonic absorption was observed for the Cu NPs reference sample. These results alone do not confirm the formation of a CuAu nanoalloy, as a mixture of Au NPs and Cu NPs would display similar absorption features. Thus, to confirm the nanoalloy nature, HRTEM analysis was conducted on the CuAu NPs sample. Figs. 2A and 2C show the lattice fringes of AuCu and Au_3Cu nanocrystallines. Most d-spacing values determined match those of the AuCu crystal phase (PDF#38-0741). However, in some locations, d-spacing values were determined to better match the Au_3Cu crystal phase (PDF#34-1302). EDX coupled with HRTEM was then employed to track the elemental mapping of a single AuCu NP. As seen in Fig. 2D, the chemical composition was analysed for each point on the red crossline that passed through an AuCu NP, being approximately 10 nm in size. From the profile of Au and Cu concentration, it can be concluded without any ambiguity that the AuCu NP is composed of Au and Cu elements with equal atomic concentration, thus consistent with the observation of the AuCu crystal phase.

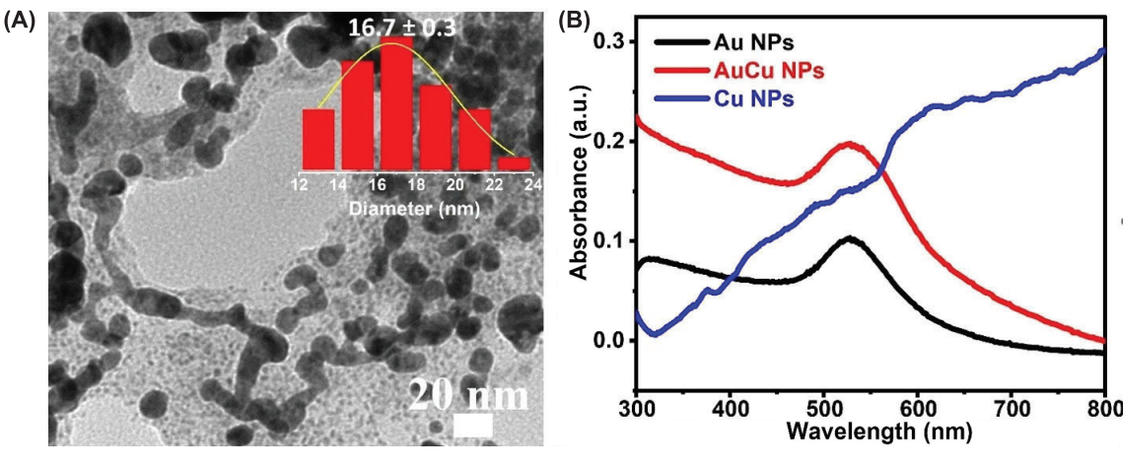

Fig. 1. (A) SEM images of the AuCu NPs. Inset shows the particle size distribution. **(B) UV-Vis spectra for a solution of AuCu NPs (red trace), Au NPs (black trace), and Cu NPs (blue trace) in DI water.**

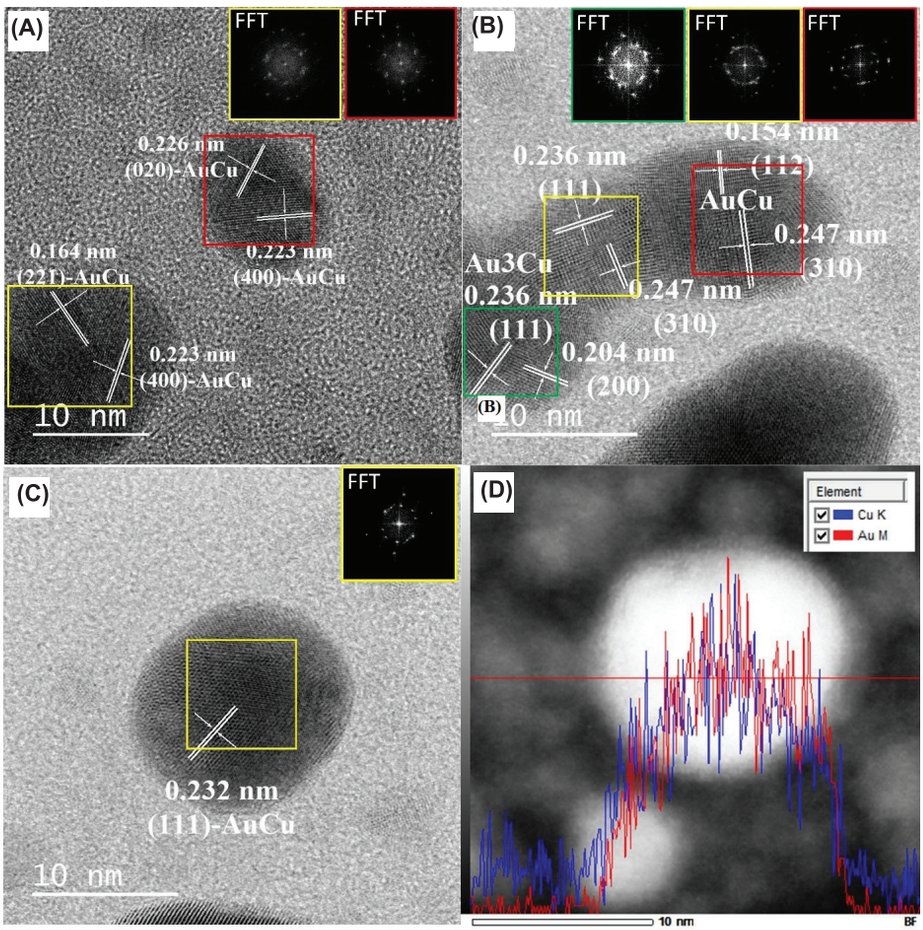

Fig. 2. (A, B, C) HR-HAADF-STEM analysis of AuCu NPs. Inset shows the corresponding FFT analysis for the region marked by the yellow square. **(D) Energy dispersive X-ray analysis along the horizontal red line.** Red and blue curves represent the Au and Cu content, respectively.

AuCu NPs were then deposited onto a graphite electrode. No additive was used to exclude potential interferences while examining the electrochemical properties of AuCu NPs. The AuCu NPs electrode was then assayed in a 0.1 M $KHCO_3$ solution saturated with CO_2 gas, at a pH of 6.8. In the first potential polarisation, a reduction event was observed at -0.4 V *vs*. RHE before the evolution of the catalytic current (Fig. 3A, black trace). However, the reduction peak vanished in subsequent potential scans (Fig. 3A, red, blue, and pink traces). We attribute this reduction event to the reduction of Cu^I or Cu^{II} species present on the surface of AuCu NPs into Cu^0. It is well known that the surface of nano Cu is spontaneously oxidised into Cu_2O and/or CuO by oxygen in the air. Hence, when handling AuCu NPs in the air, it is possible that their surface is partially oxidised, generating Cu^I, Cu^{II} oxide species. After the reduction of surface species was completed, the AuCu NPs electrode showed steady I-V curves.

The catalytic current emerged from a potential of -0.12 V *vs*. RHE. It is noted that in a neutral pH electrolyte, catalysing H_2 evolution at such a low overpotential is challenging. For example, in a pH 7 phosphate buffer electrolyte, catalytic H_2 evolution has been reported for Cu/Cu_2O with an onset potential of -0.3 V *vs*. RHE [17], Cu_2MoS_4 with an onset potential of -0.16 V *vs*. RHE [28], and amorphous CoMoS with an onset potential of -0.12 V *vs*. RHE [6, 9]. However, catalytic CO_2 reduction at such a low overpotential is rare. For example, S. Min, et al. (2016) [29] reported CO_2 reduction into CO and COOH on a Cu foam catalyst at a low potential of -0.2 V *vs*. RHE. Herein, bulk electrolysis was conducted at different potentials ranging from -0.2 to -0.9 V *vs*. RHE, and products were quantified to understand the competition between H_2 evolution and CO_2 reduction. Fig. 3B shows the evolution of the cathodic current density over 2 hours of bulk electrolysis at -0.6 V *vs*. RHE. It can

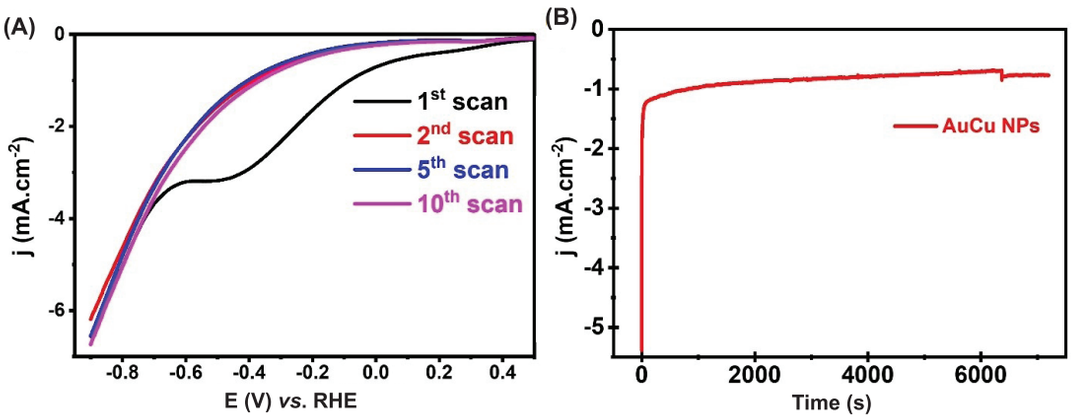

Fig. 3. Electrochemical properties of the AuCu NPs catalyst electrode. (A) Subsequent I-V curves recorded with a slow potential scan rate of 2 $mV.s^{-1}$; **(B)** I-t curve obtained when electrolysing at -0.6 V *vs.* RHE. Electrolyte was a 0.1 M $KHCO_3$ solution saturated with CO_2 (pH 6.8).

be seen that the catalytic current density slightly decreased from the initial value of -1.2 to -0.9 $mA.cm^{-2}$ over 2 hours. We attribute this decrease to the partial detachment of AuCu NPs from the graphite electrode during bulk electrolysis, which was actually observed even with the naked eye.

Gas chromatography analysis revealed the production of H_2, CO, and CH_4 (Fig. 4A). Analysis of liquid products by ion exchange chromatography demonstrated the production of HCOOH and CH_3COOH (Fig. 4B). It is important to note that the formation of other products such as C_2H_4, C_2H_5OH, etc., could not be excluded due to the limitations of experimental analysis. Figs. 4A-C show the product selectivity as a function of the applied potentials. CH_4 was produced with the highest Faradic efficiency (FE) of ~7.1% at a low cathodic potential of -0.2 V *vs.* RHE (Fig. 4A, blue trace). To the best of our knowledge, this

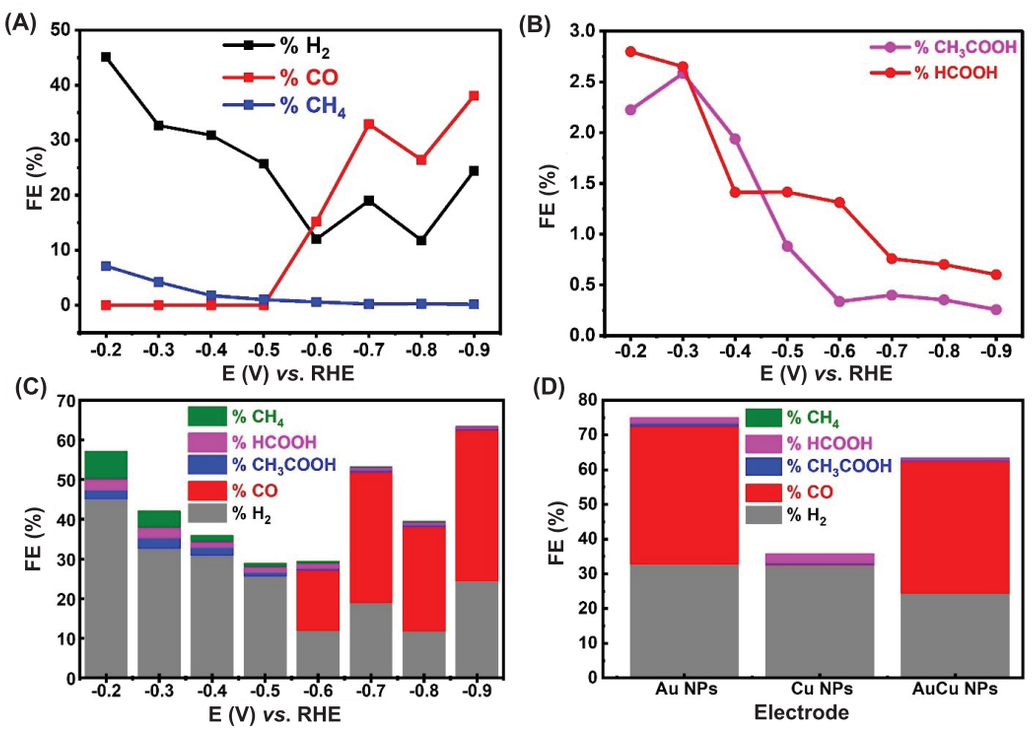

Fig. 4. Evolution of (A) gas products and (B) liquid products. (C) Product selectivity as a function of potentials applied when using the AuCu NPs catalyst electrode. (D) Comparison of products obtained at -0.9 V *vs.* Reversible hydrogen electrode using AuCu NPs, Au NPs and Cu NPs catalyst electrodes. The electrolyte was a 0.1 M $KHCO_3$ solution saturated with CO_2 (pH 6.8).

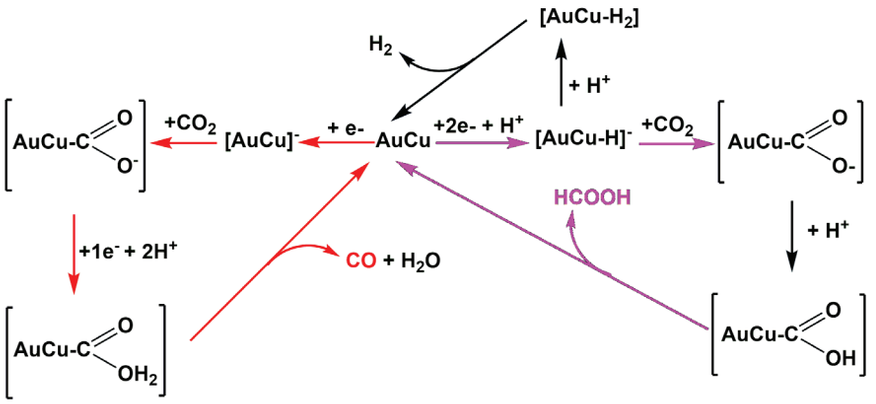

Fig. 5. Schematic illustration of competing reaction pathways on AuCu nanoparticle (NP) catalysts, leading to the formation of H_2, HCOOH, and CO products.

represents the lowest overpotential ever reported for the production of CH_4. At this potential of -0.2 V *vs.* RHE, H_2 was produced with the highest FE of 45% (Fig. 4A, black trace), while HCOOH and CH_3COOH liquid products were produced at FEs of 3.0% and 2.5%, respectively (Fig. 4A). Increasing the reducing potential caused a decrease in the production yields of H_2, HCOOH, and CH_3COOH. At -0.5 V *vs.* RHE, FE values were determined to be 26% for H_2, 1.5% for HCOOH, and 1% for CH_3COOH. At -0.6 V *vs.* RHE and higher cathodic potentials, a drastic change was observed when the production of CO occurred alongside the evolution of H_2. The production selectivity of CO increased with increasing reducing potential. At -0.9 V *vs.* RHE, CO was produced with an FE of 40%, and H_2 was produced with an FE of 25%, resulting in a molar ratio nCO/nH_2 of 1.6/1. When CO was produced, the production of HCOOH and CH_3COOH was negligible, e.g., with FEs of less than 1%. It is noted that higher CO_2-to-CO reduction selectivity, e.g., up to 85%, has been obtained for other Cu-based catalysts such as carbon-supported Cu-In nanoparticles [30]. Thus, it is critical to screen for the best metal(s) to compose Cu-based bimetallic nanoparticles capable of displaying the highest CO_2 reduction selectivity.

The currently available data clearly demonstrate the competition between the reduction of H^+ evolving H_2 and the reduction of CO_2 generating CO, HCOOH, and CH_3COOH. On the surface of the AuCu NPs catalyst, H_2 evolution proceeds through the formation of the [AuCu-H]* hydride intermediate (Fig. 5). Such a mechanism has been proposed for pure Au NPs [14] and Cu/Cu_2O NPs catalysts [17]. CO_2 molecules can bond with this hydride species, forming the [AuCu-H-CO_2]*, which is a key species for the generation of the HCOOH product (Fig. 5, pink arrow pathway). Alternatively, HCOOH can also be produced if CO_2 molecules bond directly to the reduced catalyst via an O-bond, e.g., through the formation of the [AuCu-OCO]* intermediate [31, 32]. In contrast, if CO_2 molecules bond to the reduced catalyst via a C-bond, e.g., through the formation of the [AuCu-CO_2]* species, CO is produced (Fig. 5, red arrow pathway). The progression of this pathway results in CO production (Fig. 5, red arrow pathway). Apparently, the CO production pathway was less favourable than the H_2 evolution pathway (Fig. 5, black arrow pathway). Therefore, H_2 production was prioritised at low reducing potentials. To promote CO production, a higher reducing potential was required.

To evaluate the stability of the AuCu NPs catalyst, bulk electrolysis was performed at -0.9 V *vs.* RHE for 10 hours. After electrolysis, the AuCu NPs were collected and characterised using SEM and EDX analyses. No significant morphological or compositional changes were observed (Figs. 6A, 6B), indicating the stability of the AuCu NPs catalyst during CO_2 reduction catalysis.

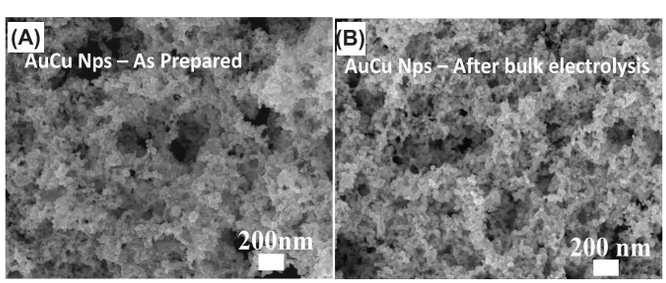

Fig. 6. SEM images of the catalyst electrode. (A) As-prepared AuCu NPs; **(B)** The same catalyst electrode after being conditioned at -0.9 V *vs.* Reversible hydrogen electrode for 10 hours in a CO_2-saturated 0.1 M $KHCO_3$ solution.

Bulk electrolysis was also conducted at -0.9 V *vs.* RHE for 2 hours using Au NPs and Cu NPs as reference samples. The Cu NPs electrode produced H_2 with an FE of 32.5% and HCOOH with an FE of 5%, but no CO was detected. In contrast, the Au NPs electrode produced H_2 and CO with almost equal FEs of 35%, resulting in a molar ratio nCO/nH_2 of approximately 1/1 (Fig. 5B). Hence, it is clear that the AuCu NPs catalyst displayed superior CO_2 reduction selectivity compared to the Au NPs and Cu NPs counterparts.

4. Conclusions

In conclusion, by employing a simple solution process, namely the chemical reduction of a Cu^{II} and Au^{III} salts mixture, AuCu nanoalloy nanoparticles (AuCu NPs) were synthesised. The AuCu NPs were crystalline and stoichiometric, with an equal atomic concentration of Au and Cu elements. AuCu NPs displayed similar plasmonic absorption properties to those of the Au NPs reference sample. In a pH 6.8 $KHCO_3$ electrolyte solution saturated with CO_2, the AuCu NPs catalysed both CO_2 reduction and H^+ reduction, evolving H_2. The products of CO_2 reduction were determined to be CO, CH_4, HCOOH, and CH_3COOH. The product selectivity was found to be dependent on the reducing potential applied. At low reduction potentials, e.g., from -0.2 to -0.5 V *vs.* RHE, the AuCu NPs catalyst promoted the production of H_2. Notably, at a low potential of -0.2 V *vs.* RHE, AuCu NPs catalysed the CO_2 to CH_4 reduction with a commendable Faradaic efficiency of 7.1%. At higher reducing potentials, e.g., from -0.6 to -0.9 V *vs.* RHE, the AuCu NPs catalyst promoted CO_2 reduction, generating CO. In comparison to Au NPs and Cu NPs monometallic catalysts, the bimetallic catalyst AuCu NPs showed superior CO_2 reduction selectivity.

CRediT author statement

Tran Duc Tien: Conducting experiment, Collecting data; Le Thi Ly: Analysing data; Nguyen Ngoc Duc: Conducting experiment, Collecting data; Nguyen Thi Quyen: Analysing data; Tran Dinh Phong: Designing research, Analysing data, Writing manuscript.

ACKNOWLEDGEMENTS

This research is funded by the Vietnam National Foundation for Science and Technology Development (NAFOSTED) under grant number 103.99-2019.328.

COMPETING INTERESTS

The authors declare that there is no conflict of interest regarding the publication of this article.

REFERENCES

[1] M.G. Walter, E.L. Warren, J.R. McKone, et al. (2010), "Solar water splitting cells", *Chemical Reviews*, **110(11)**, pp.6446-6473, DOI: 10.1021/cr1002326.

[2] M. Chatenet, B.G. Pollet, D.R. Dekel, et al. (2022), "Water electrolysis: From textbook knowledge to the latest scientific strategies and industrial developments", *Chemical Society Reviews*, **51(11)**, pp.4583-4762, DOI: 10.1039/D0CS01079K.

[3] J.N. Hansen, H. Prats, K.K. Toudahl, et al. (2021), "Is there anything better than Pt for HER?", *ACS Energy Letters*, **6(4)**, pp.1175-1180, DOI: 10.1021/acsenergylett.1c00246.

[4] P.D. Tran, T.V. Tran, M. Orio, et al. (2016), "Coordination polymer structure and revisited hydrogen evolution catalytic mechanism for amorphous molybdenum sulfide", *Nature Materials*, **15(6)**, pp.640-646, DOI: 10.1038/nmat4588.

[5] D. Merki, S. Fierro, H. Vrubel, et al. (2011), "Amorphous molybdenum sulfide films as catalysts for electrochemical hydrogen production in water", *Chemical Science*, **2(7)**, pp.1262-1267, DOI: 10.1039/C1SC00117E.

[6] D. Merki, H. Vrubel, L. Rovelli, et al. (2012), "Fe, Co, and Ni ions promote the catalytic activity of amorphous molybdenum sulfide films for hydrogen evolution", *Chemical Science*, **3(8)**, pp.2515-2525, DOI: 10.1039/C2SC20539D.

[7] H.G.S. Casalongue, J.D. Benck, C. Tsai, et al. (2014), "Operando characterization of an amorphous molybdenum sulfide nanoparticle catalyst during the hydrogen evolution reaction", *The Journal of Physical Chemistry C*, **118(50)**, pp.29252-29259, DOI: 10.1021/jp505394e.

[8] T.F. Jaramillo, K.P. Jørgensen, J. Bonde, et al. (2007), "Identification of active edge sites for electrochemical H_2 evolution from MoS_2 nanocatalysts", *Science*, **317(5834)**, pp.100-102, DOI: 10.1126/science.1141483.

[9] C.T. Nguyen, T.A. Luu, T.D. Nguyen, et al. (2023), "Exploring the sub-nanoscale structure of cobalt molybdenum sulfide and the role of a cobalt promoter in catalytic hydrogen evolution", *ACS Applied Materials & Interfaces*, **15(11)**, pp.14215-14227, DOI: 10.1021/acsami.2c20237.

[10] J.F. Callejas, C.G. Read, C.W. Roske, et al. (2016), "Synthesis, characterization, and properties of metal phosphide catalysts for the hydrogen-evolution reaction", *Chemistry of Materials*, **28(17)**, pp.6017-6044, DOI: 10.1021/acs.chemmater.6b02148.

[11] X. Chen, D. Wang, Z. Wang, et al. (2014), "Molybdenum phosphide: A new highly efficient catalyst for the electrochemical hydrogen evolution reaction", *Chemical Communications*, **50(79)**, pp.11683-11685, DOI: 10.1039/c4cc05936k.

[12] M.L. Helm, M.P. Stewart, R.M. Bullock, et al. (2011), "Electrocatalyst with a turnover frequency above 100,000 s^{-1} for H_2 production", *Science*, **333(6044)**, pp.863-866, DOI: 10.1126/science.1205864.

[13] A.L. Goff, V. Artero, B. Jousselme, et al. (2009), "From hydrogenases to noble metal-free catalytic nanomaterials for h2 production and uptake", *Science*, **326(5958)**, pp.1384-1387, DOI: 10.1126/science.1179773.

[14] T.D. Tran, M.T.T. Nguyen, H.V. Le, et al (2018), "Gold nanoparticles as an outstanding catalyst for the hydrogen evolution reaction", *Chemical Communications*, **54(27)**, pp.3363-3366, DOI:10.1039/C8CC00038G.

[15] T.D. Tran, H.V. Le, L.T. Le, et al. (2021), "Restructuring a gold nanocatalyst by electrochemical treatment to recover its H_2 evolution catalytic activity", *Sustainable Energy & Fuels*, **5(5)**, pp.1458-1465, DOI: 10.1039/D1SE00026H.

[16] T.D. Tran, L.T. Le, A.D. Nguyen, et al (2024), "Achieving excellent H_2 evolution activity of silver nanocatalyst by a simple electrochemical treatment process", *Chem. Asian J.*, **19(23)**, DOI: 10.1002/asia.202400982.

[17] J. Zhao, P.D. Tran, Y. Chen, et al. (2015), "Achieving high electrocatalytic efficiency on copper: A low-cost alternative to platinum for hydrogen generation in water", *ACS Catalysis*, **5(7)**, pp.4115-4120, DOI:10.1021/acscatal.5b00556.

[18] M.Y. Lee, K.T. Park, W. Lee, et al. (2019), "Current achievements and the future direction of electrochemical CO_2 reduction: A short review", *Critical Reviews in Environmental Science and Technology*, **50(8)**, pp.769-815, DOI: 10.1080/10643389.2019.1631991.

[19] D.N. Nguyen, E. Giannoudis, T. Straistari, et al. (2014), "Unassisted solar syngas production by a molecular dye-cobalt catalyst assembly in a tandem photoelectrochemical cell", *ACS Energy Letters*, **9(3)**, pp.829-834, DOI: 10.1021/acsenergylett.3c02480.

[20] S. Nitopi, E. Bertheussen, S.B. Scott, et al. (2019), "Progress and perspectives of electrochemical CO_2 reduction on copper in aqueous electrolyte", *Chemical Reviews*, **119(12)**, pp.7610-7672, DOI: 10.1021/acs.chemrev.8b00705.

[21] X.T. Mai, T.M. Duong, D.N. Nguyen, et al. (2025), "Sol-gel synthesis of CuO nanoparticles and its use as catalyst for electrochemical CO_2 reduction, *Energy Technology*, **13(1)**, pp.2401486, DOI: 10.1002/ente.202401486.

[22] A. Goyal, G. Marcandalli, V.A. Mints, et al. (2020), "Reduction and hydrogen evolution on a gold electrode under well-defined mass transport conditions", *Journal of The American Chemical Society*, **142(9)**, pp.4154-4161, DOI: 10.1021/jacs.9b10061.

[23] A.K. Buckley, T. Cheng, M.H. Oh, et al. (2021), "Approaching 100% selectivity at low potential on ag for electrochemical CO_2 reduction to CO using a surface additive", *ACS Catalysis*, **11(15)**, pp.9034-9042, DOI: 10.1021/acscatal.1c00830.

[24] X.Q. Wang, Q. Chen, Y.J. Zhou, et al. (2022), "Cu-based bimetallic catalysts for CO_2 reduction reaction", *Advanced Sensor and Energy Materials*, **1(3)**, DOI: 10.1016/j.asems.2022.100023.

[25] M.L. Frisch, L. Wu, C. Atlan, et al. (2023), "Unraveling the synergistic effects of Cu-Ag tandem catalysts during electrochemical CO_2 reduction using nanofocused X-ray probes", *Nature Communications*, **14(1)**, DOI: 10.1038/s41467-023-43693-2.

[26] X. Ma, Y. Shen, S. Yao, et al. (2020), "Core-shell nanoporous $AuCu_3$@Au monolithic electrode for efficient electrochemical CO_2 reduction", *Journal of Materials Chemistry A 2020*, **8(6)**, pp.3344-3350, DOI: 10.1039/C9TA09471G.

[27] J. Huang, J. Dai, J. Zhu, et al. (2020), "Bimetallic Au-Cu gradient alloy for electrochemical CO_2 reduction into C_2H_4 at low overpotential", *Journal of Catalysis*, **415**, pp.134-114, DOI: 10.1016/j.jcat.2022.09.033.

[28] P.D. Tran, M. Nguyen, S.S. Pramana, et al. (2012), "Copper molybdenum sulfide: A new efficient electrocatalyst for hydrogen production from water", *Energy & Environmental Science*, **5(10)**, pp.8912-8916, DOI: 10.1039/C2EE22611A.

[29] S. Min, X. Yang, A.-Y. Lu, et al. (2016), "Low overpotential and high current CO_2 reduction with surface reconstructed Cu foam electrodes", *Nano Energy*, **27**, pp.121-129, DOI: 10.1016/j.nanoen.2016.06.043.

[30] X. Ma, J. Tian, M. Wang, et al. (2021), "Metal-organic framework derived carbon supported Cu-In nanoparticles for highly selective CO_2 electroreduction to CO", *Catalysis Science & Technology*, **11(18)**, pp.6096-6102, DOI: 10.1039/D1CY00843A.

[31] X. Ma, Q. Wang, M. Wang, et al. (2023), "$Bi_{19}Br_3S_{27}$ nanorods for formate production from CO2 electroreduction with high efficiency and selectivity", *Chemical Engineering Journal*, **474**, DOI: 10.1016/j.cej.2023.145711.

[32] J. Wang, M. Wang, Y. Wang, et al. (2024), "Microwave-induced surface amorphization of $Cu_2(OH)_2CO_3$ catalyst promotes multi-carbon products selectivity of CO_2 electroreduction", *Science China Chemistry*, pp.1-11, DOI: 10.1007/s11426-024-2326-7.